Weight and Balance Considerations for Electrified Aircraft Propulsion Applied to the Parallel Electric-Gas Architecture with Synergistic Utilization Scheme (PEGASUS) Concept

Zachary J. Frederick* and Nathaniel J. Blaesser†
NASA Langley Research Center, Hampton, VA, 23681

Felipe Valdez‡ and Curt Hanson§
NASA Armstrong Flight Research Center, Edwards, CA, 93523

The focus of this research was to understand the impact of batteries and electric motors on the weight and balance of the Parallel Electric-Gas Architecture with Synergistic Utilization Scheme (PEGASUS) concept. Because electrified aircraft propulsion components can comprise a large part of an aircraft's weight, their integration has a significant impact on the center of gravity location and the related stability characteristics of the aircraft. We developed an analysis framework that enabled estimating the weight and volume of electrified aircraft components, their contribution to the center of gravity location, and the stability and performance of the aircraft. Trades were performed on battery placement, wing attachment point, and electric motor power to determine their impact on figures of merit such as maximum takeoff weight and block fuel. We identified batteries, and to a lesser extent electric motors, as having a large impact on aircraft center of gravity and the required horizontal tail size for longitudinal static stability. Placing electric component weight as far forward as possible resulted in reductions in the horizontal tail size required to maintain static stability. Configurations output from this framework were also evaluated using a six-degree-of-freedom simulation to quantify dynamic stability characteristics. Although shifting weight forward reduced horizontal tail size, it negatively impacted dynamic stability. This study confirms that mass property modeling and dynamic simulation, which are usually limited in conceptual design, are important for electrified aircraft concepts.

Nomenclature

CAP	=	control anticipation parameter, $g^{-1}s^{-2}$
C_{L_α}	=	lift curve slope of the wing, rad^{-1}
$C_{L_{\alpha_t}}$	=	lift curve slope of the horizontal tail, rad^{-1}
$C_{M_{\alpha_f}}$	=	rate of change of the fuselage pitching moment coefficient with angle of attack, rad^{-1}
$\bar{c}$	=	mean aerodynamic chord of the wing, ft
$c.g._{bat}$	=	longitudinal position of the battery center of gravity, measured from the nose, ft
$d\epsilon/d\alpha$	=	rate of change of tail downwash with angle of attack
L_{MLG}	=	main landing gear length, ft
l_H	=	distance between the center of gravity to the aerodynamic center of the horizontal tail, ft
l_V	=	distance between the center of gravity to the aerodynamic center of the vertical tail, ft
n_z/α	=	steady-state normal acceleration per unit change in angle of attack, g/rad
P_{BLI}	=	electric motor power of the BLI propulsor, MW
P_{ib}	=	electric motor power of the inboard propulsor, MW
P_{total}	=	total electric motor power, MW
P_{wt}	=	electric motor power of the wingtip propulsor, MW

*Aerospace Engineer, Aeronautics Systems Analysis Branch, 1 N. Dryden Street, MS 442, Hampton VA, Member
†Aerospace Engineer, Aeronautics Systems Analysis Branch, 1 N. Dryden Street, MS 442, Hampton VA, Senior Member
‡Aerospace Engineer, Dynamics and Controls Branch, P.O. Box 273, MS 4840D, Edwards, CA
§Senior Flight Controls Researcher, Dynamics and Controls Branch, P.O. Box 273, MS 4840D, Edwards, CA, Member

S = reference wing area, ft^2
S_H = horizontal tail area, ft^2
SM = static margin
S_V = vertical tail area, ft^2
T_2 = time to double, s
V_H = horizontal tail volume coefficient
V_V = vertical tail volume coefficient
x_{ac} = longitudinal position of the aircraft aerodynamic center, measured from the nose, ft
x_{np} = longitudinal position of the neutral point, measured from the nose, ft
x_w = longitudinal position of the wing, measured from the nose, ft
ζ_p = phugoid damping ratio
ζ_{sp} = short period damping ratio
η = ratio of tail to freestream dynamic pressure
θ_1 = tail strike angle, deg
θ_2 = angle between the landing gear and center of gravity with respect to the vertical, deg
λ_p = phugoid roots, s^{-1}
ω_p = phugoid natural frequency, rad/s
ω_{sp} = short period natural frequency, rad/s

I. Introduction

NASA's Aeronautics Systems Analysis Branch (ASAB) developed the Parallel Electric-Gas Architecture with Synergistic Utilization Scheme (PEGASUS) concept, shown in Fig. 1, to explore the potential benefits of electrified aircraft propulsion (EAP) technologies as applied to a regional class aircraft. The genesis of the concept was motivated by a study by Antcliff et al. [1] which demonstrated the potential for EAP enabled aircraft in the regional market. The first analysis of PEGASUS was performed by Antcliff and Capristan [2], which detailed its concept of operations (ConOps) and main design features. The aircraft's airframe is based on the 48 passenger ATR 42-500 which serves as a conventional baseline for comparing the relative benefits of EAP. Like the ATR 42-500, PEGASUS operates at a nominal cruising speed of Mach = 0.48 at an altitude of 20,000 ft.

Fig. 1 Artist's rendering of PEGASUS.

PEGASUS features three categories of propulsor: parallel hybrid-electric wingtip propulsors sized for cruise, inboard electric propulsors designed for additional thrust at takeoff, and an aft boundary layer ingestion (BLI) electric propulsor located in the tail. The aft BLI propulsor is meant to ingest and re-energize the fuselage boundary layer. The inboard propulsors and aft BLI propulsor are powered by batteries, whereas the parallel hybrid-electric turboprops are powered by a combination of batteries and fuel. The strategic location of these propulsors on PEGASUS's airframe results in propulsion-airframe integration (PAI) benefits. Figure 2 shows the location and class of each propulsor.

The hybrid-electric propulsion system allows for more flexibility in mission planning. PEGASUS was designed to perform either a 200 nmi all-electric mission or a 400 nmi hybrid-electric mission, with capacity for a reserve mission in either case [2]. Capristan and Blaesser [3] found that PEGASUS required approximately 13,000 lb of battery to satisfy these mission requirements. This battery weight is a significant percentage of maximum takeoff weight (MTOW), which is about 40,000 lb for the ATR 42-500. Previous studies did not take into account the impact of battery weight or the weight of the aft BLI propulsor on center of gravity (c.g.) location, which is constrained by stability requirements. This research sought to fill these analysis gaps.

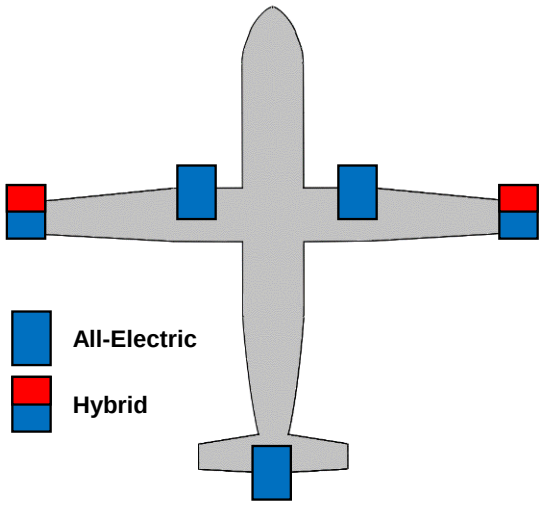

Fig. 2 PEGASUS propulsion systems.

Section II describes the development of two separate methodologies for evaluating the impact of weight and balance: a low fidelity analysis framework and a high fidelity six-degree-of-freedom (6-DOF) simulation. Section III details trade study results leveraging these two methodologies. Section IV summarizes the work performed and discusses relevant conclusions.

II. Approach

An analysis framework was developed to estimate component weights, calculate c.g., modify aircraft geometry, and evaluate aircraft performance. Figure 3 outlines the analysis framework. The individual components of the framework are described in detail in subsequent sections. The following independent variables were selected to perform trades with the framework: the longitudinal position of the battery, $c.g._{bat}$; the ratio of the BLI propulsor motor power to the total motor power, P_{BLI}/P_{total}; and the longitudinal position of the wing, x_w. For each trade, only a single parameter was varied, with the remaining two parameters fixed to a baseline value. This framework was used to perform trades on the aircraft geometry. The results of these trades were then validated using a high fidelity 6-DOF simulation.

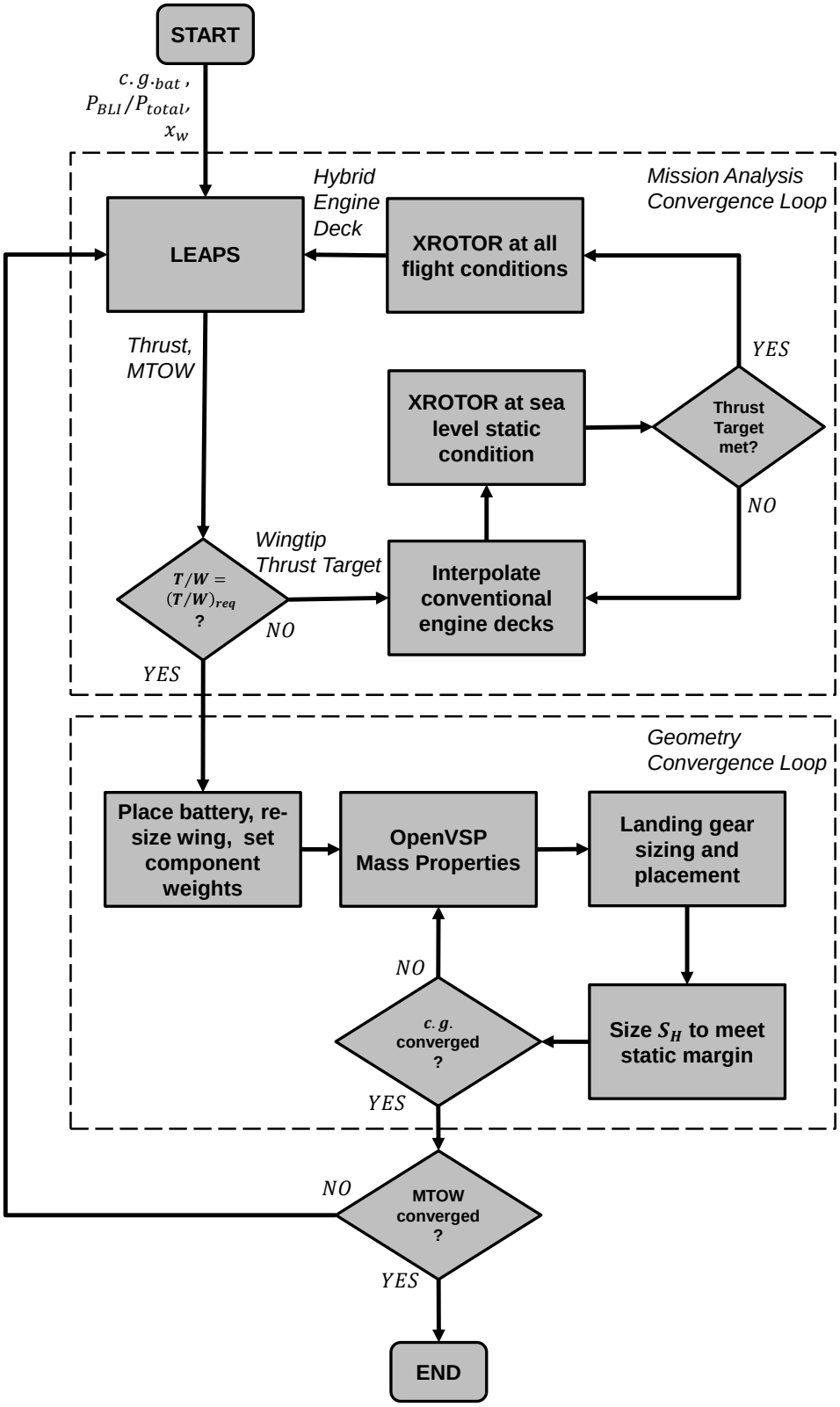

Fig. 3 Data flow diagram showing how information is passed between components in the analysis framework.

A. Mission Analysis Convergence Loop

1. Mission Analysis

The first module of the framework concerns mission analysis and propulsion system modeling. Our analysis relies heavily on the Layered and Extensible Aircraft Performance System (LEAPS) [4], a conceptual aircraft design tool written in Python which is tailored to model EAP enabled aircraft. LEAPS estimates aircraft aerodynamics, weights, and mission performance based on parameterized inputs, making it highly suitable to conceptual design. LEAPS contains empirical relations for estimating the weight of aircraft components [5], which were fed into the mass properties model. Performing a mission analysis enabled us to make comparisons between different configurations in terms of figures of merit like block fuel and block energy. In addition to the 400 nmi hybrid design mission, PEGASUS's ConOps requires the ability to perform a 200 nmi all-electric mission with sufficient reserve electric energy for a reserve mission. Finding a configuration of PEGASUS that bests meets these requirements has historically been a challenge. For this study, there is the additional complication of a mass properties model that must converge with the mission analysis results. To simplify the analysis, only PEGASUS's 400 nmi hybrid mission was considered. The goal of this study was to understand how EAP component placement impacted aircraft geometry and performance, which could still be achieved with a simpler mission definition for PEGASUS. For each configuration, thrust-to-weight ratio and wing loading were held constant at 0.435 and 70 lb/ft^2, respectively, to achieve capabilities similar to the conventional ATR 42-500.

2. Propulsion System Modeling

In order to perform the mission analysis, we needed to develop propulsion system models of the fully electric inboard and aft BLI propulsors, as well as the parallel hybrid-electric wingtip propulsor. The propulsion system is modeled within LEAPS via an engine deck, which describes the thrust and fuel/electricity consumption at every point (Mach, altitude, throttle setting) of the flight envelope. A conventional gas turbine model approximating the Pratt & Whitney PW127E was incorporated into the wingtip propulsor model for PEGASUS. This model, constructed using Numerical Propulsion System Simulation (NPSS) [6], was scaled to generate a suite of gas turbines with various sea level static shaft horsepowers (SHPs). To create a hybrid SHP engine deck, the power from the wingtip electric motor, P_{wt}, was simply added to the SHP of the gas turbine at each point in the SHP engine deck. To create fully electric SHP engine decks, it was assumed that available electric motor power was constant throughout the flight envelope and did not lapse with altitude.

XROTOR [7], an open-source propeller design and analysis tool, was used to compute thrust from the SHP at each flight condition. XROTOR was used to design a propeller based on minimum induced loss for each propulsor, using the power available at top of climb (TOC) as the design condition. XROTOR was then executed in analysis mode at each point in the SHP engine deck to generate a thrust engine deck.

A convergence loop was used to implement the constant thrust-to-weight ratio sizing. For each configuration, the electric motor sizes were all fixed, so the only means of varying thrust was to scale the gas turbine portion of the parallel hybrid-electric wingtip propulsor. After each LEAPS execution, the thrust-to-weight ratio at takeoff was recorded, as well as the sea level static thrusts of each propulsor. Using this information, an optimizer selected a thrust target for the wingtip propulsor in order to meet the overall thrust-to-weight ratio. Another solver was used to find the SHP of the gas turbine which produced that thrust target by interpolating between the conventional SHP engine decks and evaluating sea level static thrust using XROTOR. Once the desired thrust target was met, XROTOR was repeatedly called to generate the entire hybrid engine deck, which was fed back to LEAPS. This process was repeated until the desired thrust-to-weight ratio was achieved. This process is represented by the upper dashed box entitled "Mission Analysis Convergence Loop" within Fig. 3.

B. Geometry Convergence Loop

1. Mass Properties Model

The results of the converged mission analysis module were passed to a geometry convergence loop, represented by the lower dashed box entitled "Geometry Convergence Loop" within Fig. 3. OpenVSP [8], a parametric aircraft geometry tool, was used to model the aircraft geometry. Since the inputs into OpenVSP are parameterized, automated modification of the aircraft geometry was enabled via the Python API. Python was used as the interface between LEAPS, OpenVSP, and custom scripts. Figure 4 illustrates the internal components of the mass properties model.

Electrical component power density and efficiency assumptions were informed by proprietary industry data [9].

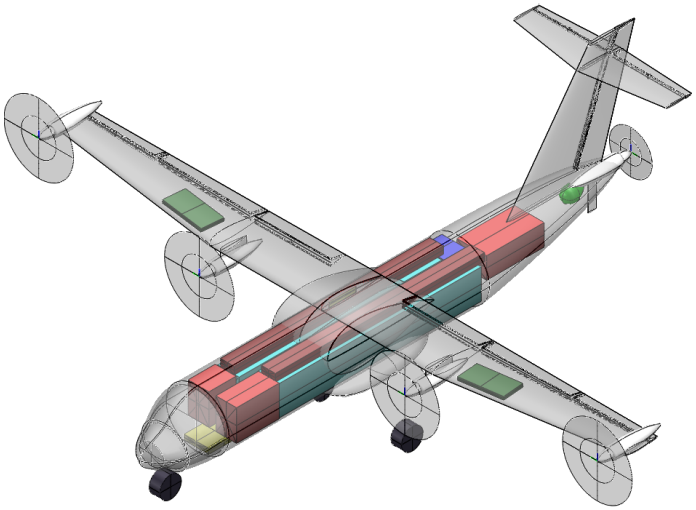

Fig. 4 Mass properties OpenVSP model detailing colorized internal components.

This allowed the weight of the electric powertrain to be estimated for each motor power. Weight estimates for other components such as the fuselage, wing, and empennage were calculated by LEAPS. These weights were then applied to each component within the mass properties model. All components were modeled as being of uniform density, with the exception of the wing and fuselage, which were modeled as thin shells. Some items from the LEAPS weight statement were not modeled explicitly but grouped with larger components. For example, the avionics and instruments weights were applied to a single conformal cockpit component. The mass properties toolbox within OpenVSP was used to compute the volume of components, moments of inertia, and c.g. location.

The battery was modeled as a single pack placed under the passenger compartment of the fuselage. The energy requirement from the LEAPS mission analysis and the total system efficiency of the electrical system were used to determine the battery weight required. A battery specific energy (BSE) of 500 W-hr/kg was assumed. The discharge of the battery was limited to 80% of its capacity to avoid damaging the battery. Since the height and width of the battery pack were fixed by the fuselage geometry, the length of the pack was used to meet the required battery size. The c.g. location of the battery was an independent variable constrained by forward and aft limits imposed by the fuselage outer mold line (OML). The density of the battery was assumed to be 2 kg/L [9]. For the levels of electrification considered in this study, all batteries were able to be stored in the underfloor compartment of the fuselage without resorting to storing batteries within the wing.

2. Landing Gear Sizing and Placement

The main landing gear placement is based on two user-specified angles, the c.g. location, and the OML of the fuselage. Figure 5 shows the two user-specified angles where θ_1 is the tail strike angle and θ_2 is the angle between the landing gear and c.g. with respect to the vertical. Raymer [10] suggests $\theta_2 \approx 15°$ to prevent tip-over. As implied by its name, θ_1 is the maximum pitch angle the vehicle can maintain during takeoff and landing without striking the tail on the runway. Higher angles give the pilot more margin to operate the aircraft but lead to longer landing gear. Typical ranges for θ_1 on commercial aircraft are 10 to 15°. For this study, we selected a θ_1 of 15°.

The location on the aft fuselage where a tail strike occurs varies with landing gear position. The analysis includes a polynomial fit of the aft fuselage so that we can calculate the angle tangent to any point via taking the derivative of the polynomial. The tail strike constraint defines a line tangent to the aft fuselage at an angle θ_1 with respect to the horizontal. Likewise, the θ_2 constraint defines another line running through the c.g. location on which the main landing gear must be placed. Given these two equality constraints, there exists only one acceptable main landing gear position, which varies as a function of c.g. position.

A weakness of this methodology was that we did not account for the presence of the aft BLI propulsor when determining tail strike angle. Depending on the propeller diameter, it is likely that the propeller blade would supersede the underside of the fuselage as the location of a tail strike. It may be possible to eliminate this consideration by using a

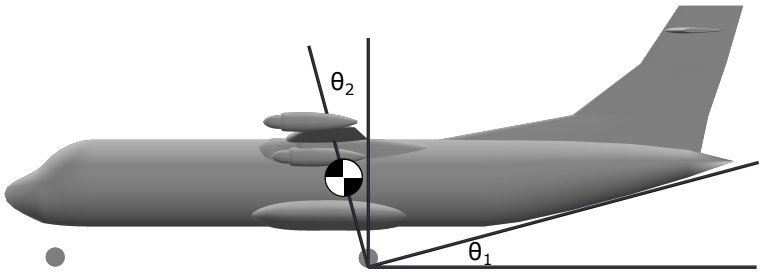

Fig. 5 The required angles for main landing gear placement.

two-bladed propeller that can be locked horizontally during takeoff and landing, as long as the thrust of the aft BLI propulsor is not required. Since such an approach was not considered for this study, it is likely that the main landing gear must be lengthened to account for the aft BLI propulsor.

The nose gear placement is less critical at the conceptual design level as it is tied to fewer requirements, primarily wheel base and the percentage of weight on the nose gear. Both requirements are important for ground handling but do not drive other parts of the aircraft's configuration at this stage. Because of this, we placed the nose gear under the cockpit and did not alter its position during the main landing gear placement.

3. Tail Sizing

Typically for conceptual design, the horizontal tail is sized using empirical volume coefficients from similar aircraft. This method does not explicitly take into account one of our independent variables, x_w (except for its influence on c.g.), and was therefore ill-suited for this study. In order to maintain similar longitudinal stability characteristics, we decided to hold static margin fixed between configurations and use this requirement to size the horizontal tail. We evaluated static margin at the full fuel and maximum payload loading condition and did not consider how it varied with different loading conditions. Since positive static margins of 5 to 10% are common for transport aircraft [10], we fixed static margin at this loading condition at 10%. A limitation of this method is that it does not take into account other sizing considerations, such as whether the horizontal tail provides sufficient pitching moment to trim the aircraft at a reasonable angle of attack. It also does not consider the control effectiveness of the elevator and its ability to provide sufficient pitch control for maneuverability.

The relationship between static margin, neutral point, and c.g. is defined by Eq. (1). Given the c.g. location of the aircraft, and holding wing location fixed, the neutral point position was adjusted by scaling the horizontal tail area to meet the static margin requirement. A semi-empirical method presented by Caughey [11] was used for estimating the neutral point as a function of only the aircraft geometry. This is represented by Eq. (2). We assumed the ratio of tail to freestream dynamic pressure, η, was one. PEGASUS has a T-tail configuration so it is reasonable to assume the horizontal stabilizer sees relatively undisturbed flow during steady level flight. Details for estimating lift curve slopes, downwash, and fuselage moment contributions are contained within Caughey's report.

$$SM = \frac{x_{np}}{\bar{c}} - \frac{x_{cg}}{\bar{c}} \tag{1}$$

$$\frac{x_{np}}{\bar{c}} = \frac{x_{ac}}{\bar{c}} + \eta V_H \frac{C_{L_{\alpha_t}}}{C_{L_\alpha}}\left(1 - \frac{d\epsilon}{d\alpha}\right) - \frac{C_{M_{\alpha_f}}}{C_{L_\alpha}} \tag{2}$$

The horizontal tail volume coefficient, V_H, has its standard definition in Eq. (3) where S is the wing area, $\bar{c}$ is the wing mean aerodynamic chord (MAC), S_H is the horizontal tail area, and l_H is the distance from the c.g. to the aerodynamic center of the horizontal tail. The aerodynamic centers of the wing, horizontal tail, and vertical tail were assumed to be at 25% of their respective MAC [10]. Vertical tail sizing was achieved through a constant vertical tail volume coefficient, V_V, which is described by Eq. (4) where S_V is the vertical tail area and l_V is the distance from the c.g. to the aerodynamic center of the vertical tail. This was held to a value of 0.102 to be comparable to the conventional ATR 42-500.

$$V_H = \frac{S_H l_H}{S\bar{c}} \tag{3}$$

$$V_V = \frac{S_V l_V}{S\bar{c}} \tag{4}$$

C. 6-DOF Non-linear Flight Simulation

A time-based simulation of the PEGASUS aircraft was developed to support static and dynamic flight stability analyses of various design permutations. Applied aerodynamic and propulsive forces, along with mass property characteristics, are input to a set of non-linear, 6-DOF equations of motion to calculate linear and rotational accelerations. The simulation determines trimmed aerodynamic angles, flight control deflections, and thrust settings for a specific flight condition. Once trimmed, the simulation outputs a linearized model of the aircraft dynamics for flying qualities (FQs) analysis and flight control design. A brief overview of the simulation models is given below.

1. Mass Properties

The PEGASUS simulation mass properties model is a two-dimensional lookup table of mass, center of gravity, and moments and products of inertia for any combination of fuel load and passenger load. The tables are built using the Mass Properties analysis tool in OpenVSP. Subsystem weights from LEAPS are assigned to model components within OpenVSP as uniform density or thin shell elements.

2. Aerodynamics

The PEGASUS aerodynamics model is a three-dimensional lookup table of aerodynamic coefficients (lift, drag, stability and control derivatives) versus airspeed, altitude, and angle of attack. The VSPAERO vortex-lattice method (VLM) within OpenVSP was used to compute these aerodynamic coefficients. It is important to note that VSPAERO does not predict viscous effects on lift and drag and ignores stalling effects for large angles of attack. The OpenVSP Parasite Drag tool was used to approximate the parasitic drag of the aircraft. Propeller-induced aerodynamic effects were assumed to be zero for simplicity, although isolated thrust force and moment contributions were included.

3. Flight Control

The distributed electric propulsion (DEP) nature of the PEGASUS concept introduces the possibility of using thrusters for flight control. For this analysis, however, the flight control design relies on traditional control effectors and symmetric thrust. Stability augmentation is added in the form of a yaw damper. The pilot is modeled using a classical proportional-integral-derivative (PID) controller. The elevator adjusts pitch attitude in order to achieve the desired climb rate. Forward speed is maintained via changes in the thrust setting. Heading changes are accomplished using bank-to-turn with a feed-forward rudder command for turn coordination.

4. Propulsion System

The propulsion model includes the thrust of each propulsor, the related pitching and yawing moments due to offsets from the c.g., and torque contributions to the aircraft rolling moment. PAI effects such as BLI and wingtip vortex cancellation are not modeled and are not expected to have a significant effect on static or dynamic stability.

III. Results

A baseline configuration for PEGASUS was selected for which trades on battery placement, motor size, and wing location were analyzed. This baseline was not based on past sizing efforts for PEGASUS and was simply an arbitrary starting point from which to perform these trades. The battery was placed in the forward-most position, because moving the c.g. forward was *a priori* known to result in the smallest required horizontal tail area for a given static margin. Inboard propulsor motor power, P_{ib}, was a constant 0.2 MW for all configurations. The remaining motor power for the baseline was equally split between the wingtip and BLI propulsor classes, resulting in a P_{wt} of 0.25 MW and a P_{BLI} of 0.5 MW, for a P_{BLI}/P_{total} of 36%. The baseline wing position was approximately the same location as the conventional ATR 42-500.

A. Battery Placement

From the baseline configuration, the longitudinal position of the battery was varied from the forward-most possible position to the aft-most. Since the battery constituted the majority of the total EAP component weight at around 8,000 lb, its location had a significant impact on the aircraft's c.g. location. This aft shift in c.g. required a one-to-one shift in neutral point to maintain static margin, necessitating an increase in horizontal tail area. It is important to note that wing location was fixed for this trade and that shifting the wing aft would help mitigate this increase in horizontal tail area.

Shifting the c.g. aft also reduced l_v. This required an increase in S_V to maintain a constant V_V, per Eq. (4). Figure 6 shows the impact on horizontal and vertical tail area that resulted from shifting the battery pack aft.

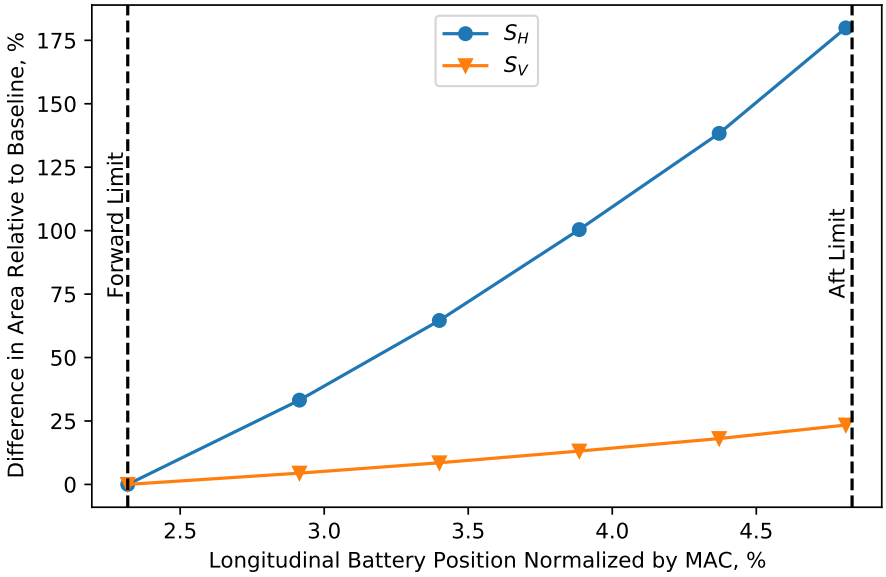

Fig. 6 Impact of change in battery position on horizontal and vertical tail area.

Another effect of shifting weight further aft was a slight reduction in main landing gear length, L_{MLG}. Since the placement of the main landing gear is fully defined by the c.g. position, shifting the c.g. aft also moves the main landing gear aft and slightly upward, so that it continues to lie on the line tangent to the fuselage which enforces the tail strike angle constraint. This reduction in landing gear length has the benefit of reduced landing gear weight; however, this effect is small and overshadowed by the increased weight and drag of the larger empennage. This is clearly shown in Fig. 7, where performance metrics like block fuel and block energy increased as the battery was shifted aft, despite the reduction in landing gear length.

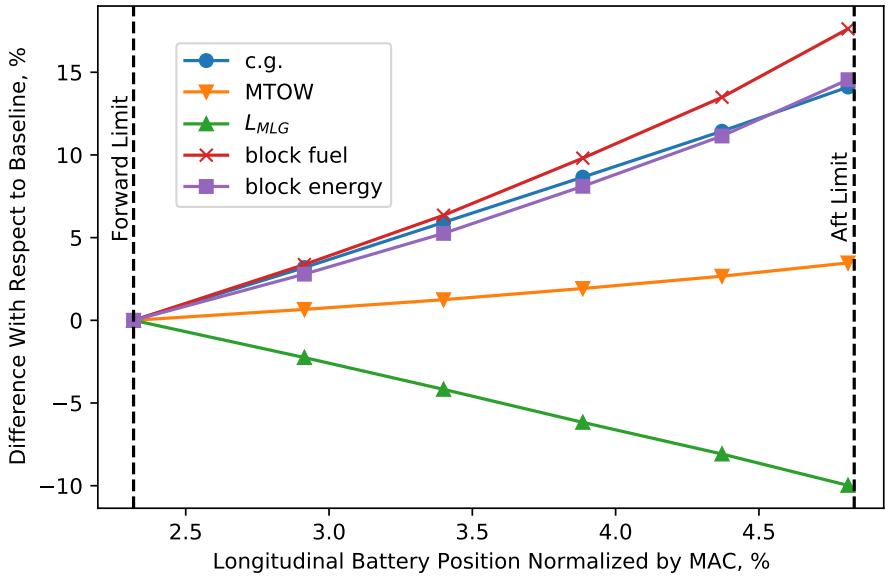

Fig. 7 Impact of battery position on various figures of merit.

B. Motor Size

The next trade involved varying the allocation of electric motor power to the BLI propulsor. For the configurations considered, the total motor power was held constant so that the electric energy used and battery weight were nearly constant. The power of the inboard propulsors was also fixed, so this trade resulted in a shift in motor power between the wingtip and BLI propulsors. Increasing the motor power allocated to the aft BLI propulsor had the effect of shifting the aircraft c.g. aft, requiring an increase in horizontal tail area to meet static margin. Figure 8 shows how S_H and S_V vary. This is the same effect observed from shifting battery weight aft; however, the effect is less severe because the weight of the electric propulsors was much less than the weight of the battery pack.

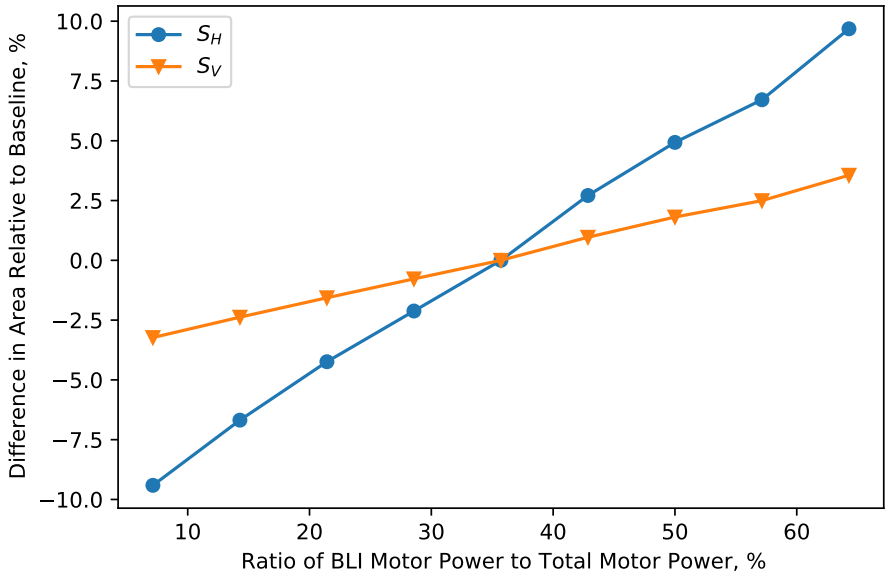

Fig. 8 Impact of motor allocation on horizontal and vertical tail area.

Figure 9 shows the impact of shifting motor power on c.g., MTOW, L_{MLG}, block fuel, and block energy. One interesting result is a local minimum in block fuel and block energy occurring near the baseline configuration. There are two competing trends producing this result. Decreasing the share of motor power allocated to the aft BLI propulsor increases the thrust loading of the wingtip propulsors, which reduces the propulsive efficiency of the entire system [12] and increases block fuel and block energy. The other trend resulting from increasing aft BLI propulsor power is the previously discussed aft shift in c.g., resulting in increased S_H and MTOW, requiring greater energy consumption to complete the mission.

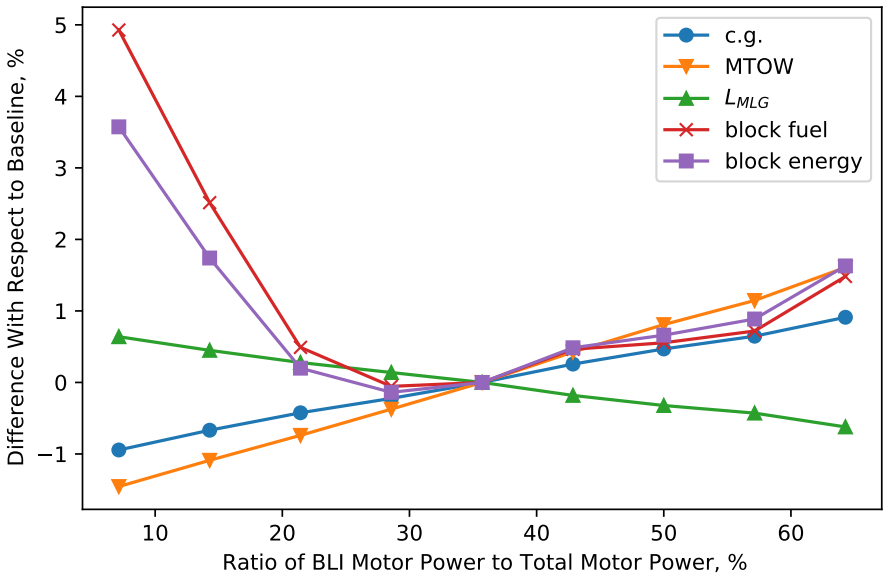

Fig. 9 Impacts of shifting motor power to the aft BLI propulsor.

C. Wing Placement

The final trade considered was shifting the longitudinal position of the wing. The main impacts of this were changing the c.g. location, which altered the moment arm of the horizontal tail, and changing the location of the aircraft's aerodynamic center. Both of these trends fed into the estimation for neutral point location, with the altered aerodynamic center location having the most impact. The net result was a decrease in horizontal tail area for wing positions shifted aft of the baseline position. Even small changes in wing position had outsized impacts on horizontal tail area. For example, shifting the wing aft by 20% of MAC resulted in a nearly 50% decrease in horizontal tail area. Figure 10 shows how S_H and S_V traded with wing position, and Fig. 11 shows how other figures of merit traded.

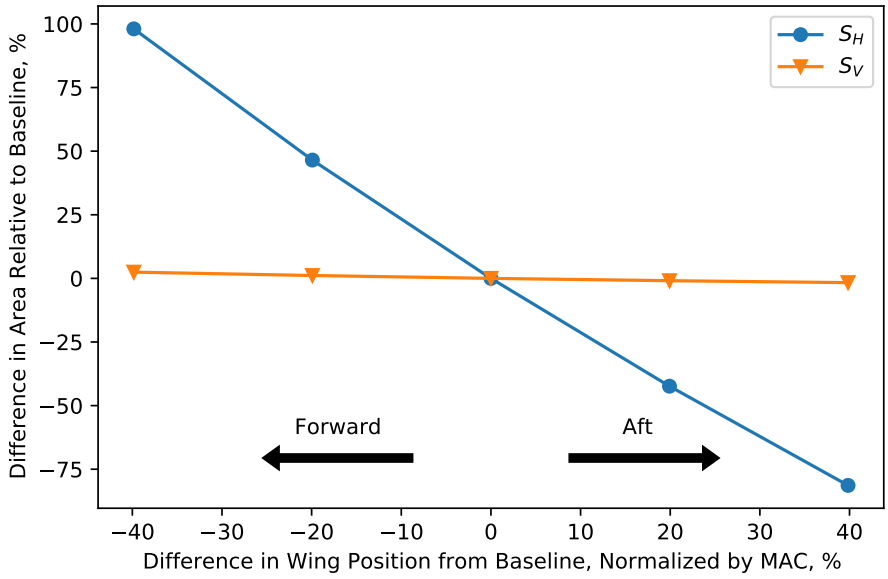

Fig. 10 Change in tail area with change in wing position.

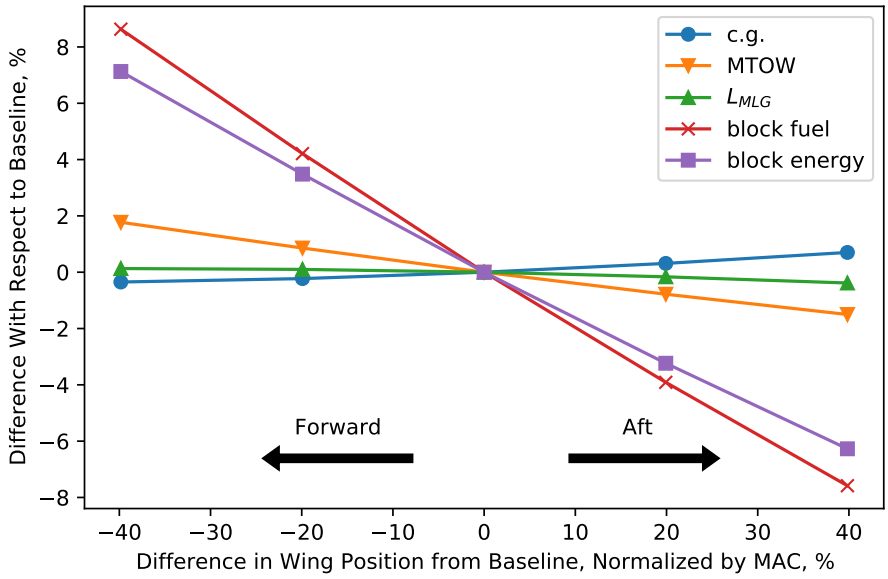

Fig. 11 Effect of shifting longitudinal wing position on various figures of merit.

D. 6-DOF Analysis

The PEGASUS design team developed aircraft linear models and a 6-DOF time-based simulation to evaluate the impacts of design choices on the dynamic stability and FQs of the PEGASUS airplane. Mass properties, aerodynamics, and propulsion models from the team's conceptual design tools were integrated using the MathWorks SIMULINK simulation software [13]. The PEGASUS simulation was used to trim the aircraft at a specified flight condition and output linear models for FQs analysis and autopilot design. FQs criteria are taken from MIL-STD-1797B [14] and MIL-8785C [15]. For a transport aircraft, Level 1 FQs are desirable, Level 2 FQs are marginally acceptable, and Level 3 FQs are unacceptable.

Three configurations generated from the previously discussed framework were evaluated using the 6-DOF simulation. In addition to the baseline, two edge cases were evaluated, with motor power and battery placement varied in order to shift weight to the most forward or most aft position. Among all three configurations, wing placement and total motor power were held constant. A summary of the three cases (baseline, aft biased, and forward biased) is presented as Table 1.

Table 1 Three Configurations Evaluated Using the 6-DOF Simulation

Configuration	P_{wt}, MW	P_{ib}, MW	P_{BLI}, MW	$c.g._{bat}/\bar{c}$
Baseline	0.25	0.2	0.5	2.3
Aft Biased	0	0.2	1.0	4.4
Forward Biased	0.5	0.2	0	2.3

1. Longitudinal Analysis

An assessment of the longitudinal FQs includes calculation of the pitch static margin as well as the phugoid and short period mode frequency and damping. The tail was initially sized for a 10% static margin using the semi-empirical method described previously. VSPAERO lift and pitching moment coefficients at two angles of attack were used to compute the static margin, which is proportional to the change in pitching moment with respect to the change in lift. Calculations using VSPAERO indicate that the semi-empirical method tends to under-predict the static margin for PEGASUS. Table 2 shows a comparison of the static margins of the three PEGASUS configurations as calculated from VSPAERO.

Table 2 Static Margin Comparison of PEGASUS Variants at 4° Angle of Attack

	Static Margin	
Configuration	Goal	VSPAERO
Baseline	10%	23%
Aft Biased	10%	38%
Forward Biased	10%	23%

For each of the three PEGASUS variants, the phugoid mode is very lightly damped but stable. Table 3 shows that all three variants are Level 2 based on the MIL-F-8785C criteria for the phugoid mode. Within Table 3, T_2 is the time to double, as defined in Eq. (5). Within Eq. (5), λ_p are the phugoid roots, ω_p is the phugoid natural frequency, and ζ_p is the phugoid damping ratio. The control anticipation parameter (CAP) is a commonly used metric for aircraft short period FQs which is defined in Eq. (6) where ω_{sp} is the short period natural frequency and n_z/α is the steady-state normal acceleration per unit change in angle of attack.

$$T_2 = \frac{ln(2)}{|\zeta_p|\omega_p} \text{ for } \lambda_p < 0 \tag{5}$$

$$CAP = \frac{\omega_{sp}^2}{n_z/\alpha} \tag{6}$$

Figure 12 illustrates the MIL-STD-1797B short period FQs criteria for aircraft in cruise flight (Category B) as the relationship between CAP and short period damping ratio, ζ_{sp}. All three PEGASUS configurations meet Level 1 criteria but with the baseline and forward biased cases closer to Level 2 boundaries on both the frequency and damping axes. Changes to the vehicle design that reduce short period damping or natural frequency, such as a decrease in horizontal tail size or an increase in pitch intertia, could drop the short period mode into Level 2, which would be adequate to accomplish the mission but with some increase in the pilot's workload.

Table 3 MIL-F-8785C Longitudinal Damping Ratio Criteria

	Phugoid Damping Ratio			
	MIL-F-8785C Criteria	Baseline	Aft Biased	Forward Biased
Level 1	$\zeta_p \geq 0.04$			
Level 2	$\zeta_p \geq 0$	0.0239	0.0294	0.0244
Level 3	$T_2 \geq 55$ *seconds*			

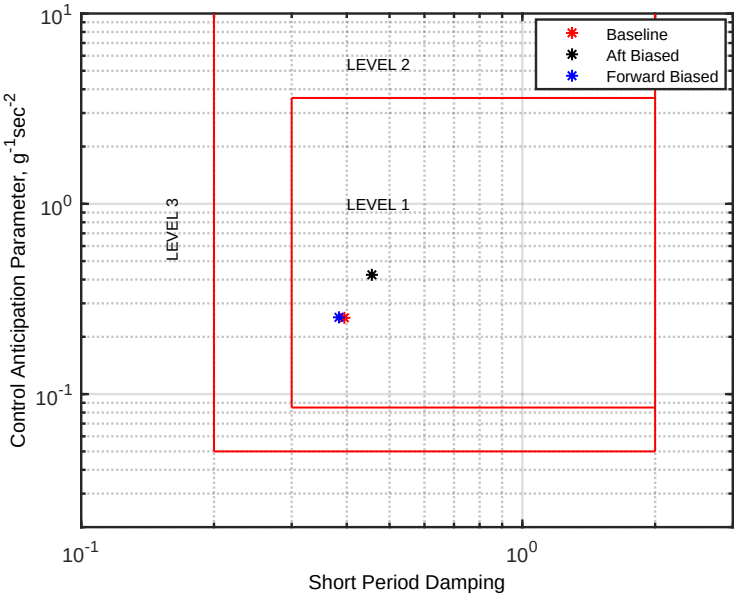

Fig. 12 Short period flying qualities prediction of PEGASUS variants.

2. Lateral-Directional Axes

Lateral-directional FQs are described by the Dutch roll, spiral, and roll subsidence modes. For the three PEGASUS configurations considered, these modes were stable; however, time history simulations revealed a highly oscillatory vehicle response in the lateral-directional axis. Stability augmentation was added in the form of a yaw damper using the yaw rate of the aircraft to command the rudder control surface to move so the yaw oscillations are damped faster than naturally. This counteracts the Dutch roll aerodynamic mode of the aircraft. Figure 13 shows that the Dutch roll modes of all three configurations were marginally Level 2, and that the addition of a yaw damper provided Level 1 FQs. However, careful consideration needs to be paid to the bare airframe Dutch roll mode, as a malfunction of the yaw damper could cause severe oscillations leading to irrecoverable loss of control [16].

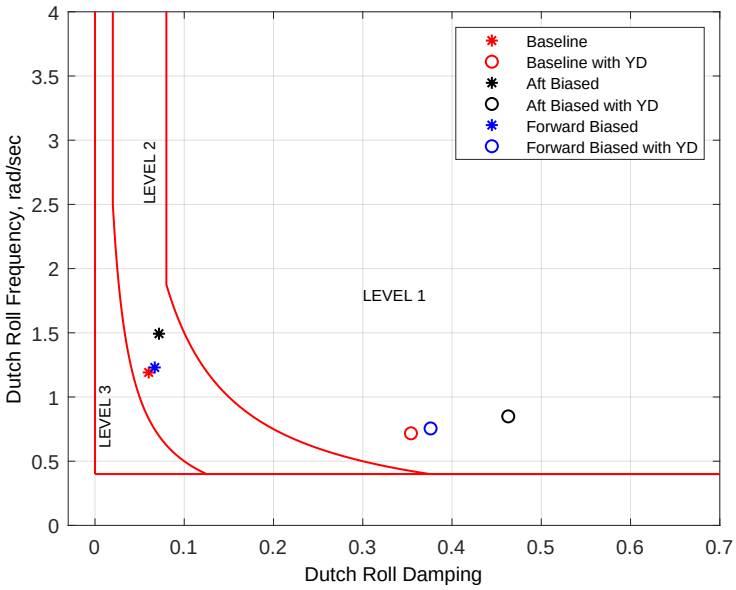

Fig. 13 Dutch roll frequency versus damping criteria for Category B.

IV. Concluding Remarks

We developed a framework for evaluating the impact of EAP components on c.g. and related stability characteristics. We found that battery placement has a significant impact on c.g., and to minimize horizontal tail area, the battery should be placed as far forward as possible. The impact of the aft BLI propulsor on c.g., and subsequent tail size, was found to be less important than its impact to propulsive efficiency, in terms of block fuel and block energy. Shifting the wing location aft resulted in a reduction in horizontal tail size when considering static margin as the only sizing criteria. This method of sizing the horizontal tail did not consider whether the aircraft could actually trim at a reasonable angle of attack during cruise or whether the elevator provided sufficient control effectiveness. Because of this, the framework suggests that the horizontal tail could be eliminated while still achieving a static margin of 10%, which is not realistic given these other considerations. In future work, we plan to improve our methodology for horizontal tail sizing by considering the full range of possible loading conditions and ensuring the aircraft can be trimmed and has sufficient controllability across the entire c.g. envelope.

This parametric study only considered isolated changes to battery placement, motor size, and wing placement. Holding everything fixed and varying one variable at a time was not representative of the actual aircraft design process, but it was useful for testing the capabilities of the framework and getting a sense of the relative influence of each parameter. An area for future work will be to optimize the selection of these parameters for a configuration of PEGASUS that minimizes figures of merit such as block fuel or block energy.

These results confirm the importance of weight and balance and stability considerations in conceptual aircraft design, especially for EAP enabled concepts. Mass properties modeling is usually limited at the conceptual design stage, but it is necessary for unconventional concepts such as those employing EAP. This study did not consider PAI which is fundamental to the design of PEGASUS and is expected to offer additional performance benefits. We plan to integrate computational fluid dynamics (CFD) surrogate models into the framework so that we can bookkeep PAI benefits in addition to weight and balance impacts of different propulsor configurations.

We also found that careful consideration needs to be given to dynamic stability when performing design tradeoff studies, particularly those involving mass distribution and aerodynamic surface sizing. Although all three configurations evaluated with the 6-DOF simulation were dynamically stable, the phugoid and Dutch roll modes displayed less than desirable Level 2 FQs which can be improved by modifying the aircraft geometry. Identifying poor FQs or flight dynamics instabilities early in the aircraft design may have a significant positive impact on the later design phases. Integration of high-fidelity aircraft simulation models in early aircraft design can potentially uncover key aspects that drive the aircraft design process.

V. Acknowledgments

The authors thank Jesse Quinlan, Ty Marien, and Mark Guynn for their guidance and input. The NASA Advanced Air Transport Technology (AATT) project funded this research.

References

[1] Antcliff, K. R., Guynn, M. D., Marien, T., Wells, D. P., Schneider, S. J., and Tong, M. J., "Mission Analysis and Aircraft Sizing of a Hybrid-Electric Regional Aircraft," No. 2016-1028 in AIAA SciTech Forum, American Institute of Aeronautics and Astronautics, 2016. doi:10.2514/6.2016-1028, URL https://doi.org/10.2514/6.2016-1028.

[2] Antcliff, K. R., and Capristan, F. M., "Conceptual Design of the Parallel Electric-Gas Architecture with Synergistic Utilization Scheme (PEGASUS) Concept," No. 2017-4001 in AIAA AVIATION Forum, American Institute of Aeronautics and Astronautics, 2017. doi:10.2514/6.2017-4001, URL https://doi.org/10.2514/6.2017-4001.

[3] Capristan, F. M., and Blaesser, N. J., "Analysis of the Parallel Electric-Gas Architecture with Synergistic Utilization Scheme (PEGASUS) Concept," NASA Technical Memorandum NASA/TM–2019–220396, NASA, Aug. 2019. URL https://ntrs.nasa.gov/citations/20190030874.

[4] Welstead, J. R., Caldwell, D., Condotta, R., and Monroe, N., "An Overview of the Layered and Extensible Aircraft Performance System (LEAPS) Development," No. 2018-1754 in AIAA SciTech Forum, American Institute of Aeronautics and Astronautics, 2018. doi:10.2514/6.2018-1754, URL https://doi.org/10.2514/6.2018-1754.

[5] Wells, D. P., Horvath, B. L., and McCullers, L. A., "The Flight Optimization System Weights Estimation Method," NASA Technical Memorandum NASA/TM-2017-219627/Volume I, NASA, 2017. URL https://ntrs.nasa.gov/citations/20170005851.

[6] Jones, S., "An Introduction to Thermodynamic Performance Analysis of Gas Turbine Engine Cycles Using the Numerical Propulsion System Simulation Code, Computing Systems in Engineering," NASA Technical Memorandum NASA/TM–2007-214690, NASA Glenn Research Center, 2007. URL https://ntrs.nasa.gov/citations/20070018165.

[7] Drela, M., and Youngren, H., "XROTOR Download Page," Online, Feb. 2011. URL http://web.mit.edu/drela/Public/web/xrotor/.

[8] Gloudemans, J., Davis, P., and Gelhausen, P., "A rapid geometry modeler for conceptual aircraft," No. 96-0052 in 34th Aerospace Sciences Meeting and Exhibit, American Institute of Aeronautics and Astronautics, 1996. doi:10.2514/6.1996-52, URL https://doi.org/10.2514/6.1996-52.

[9] Marien, T. V., Blaesser, N. J., Frederick, Z. J., Guynn, M. D., Kirk, J. T., Fisher, K., Schneider, S., Thacker, R. P., and Frederic, P., "Methdology Used for an Electrified Aircraft Propulsion Design Exploration," Submitted for publication, 2021.

[10] Raymer, D. P., *Aircraft Design: A Conceptual Approach*, AIAA Education Series, 2012.

[11] Caughey, D. A., "Introduction to Aircraft Stability and Control Course Notes for M&AE 5070," Online, 2011. URL https://courses.cit.cornell.edu/mae5070/Caughey_2011_04.pdf.

[12] Blaesser, N. J., "Propeller-Wing Integration on the Parallel Electric-Gas Architecture with Synergistic Utilization Scheme (PEGASUS) Aircraft," No. 2019-1809 in AIAA SciTech Forum, American Institute of Aeronautics and Astronautics, 2019. doi:10.2514/6.2019-1809, URL https://doi.org/10.2514/6.2019-1809.

[13] Simulink Documentation, "Simulation and Model-Based Design," Online, Accessed June 2021. URL https://www.mathworks.com/products/simulink.html.

[14] "Flying Quantities of Piloted Aircraft," Military Specification MIL-STD-1797, Department of Defense, 2006.

[15] "Military Specification Flying Qualities of Piloted Airplanes," Military Specification MIL-F-8785C, Department of Defense, 1980.

[16] "Boeing 737 Postmaintenance Test Flight Encounters Uncommanded Roll-and-Yaw Oscillations," *Flight Safety Foundation*, Vol. 55, No. 5, 1998, pp. 1–8.